



# 1 Secondary Aerosol Formation in Incense Burning Particles by 2 Ozonolysis and Photochemical Oxidation

3  
4 Zhancong Liang<sup>1,2</sup>, Liyuan Zhou<sup>1,2</sup>, Xinyue Li<sup>1</sup>, Rosemarie Ann Infante Cuevas<sup>1,2</sup>, Rongzhi Tang<sup>1,2</sup>, Mei  
5 Li<sup>3,4</sup>, Chunlei Cheng<sup>3,4</sup>, Yangxi Chu<sup>5</sup>, Chak K. Chan<sup>1,2,6\*</sup>

6  
7 <sup>1</sup> School of Energy and Environment, City University of Hong Kong, Hong Kong, China

8 <sup>2</sup> City University of Hong Kong Shenzhen Research Institute, Shenzhen, China

9 <sup>3</sup> Institute of Mass Spectrometry and Atmospheric Environment, Guangdong Provincial Engineering Research Center for On-  
10 line Source Apportionment System of Air Pollution, Jinan University, Guangzhou 510632, China

11 <sup>4</sup> Guangdong-Hongkong-Macau Joint Laboratory of Collaborative Innovation for Environmental Quality, Guangzhou 510632,  
12 China

13 <sup>5</sup> State Key Laboratory of Environmental Criteria and Risk Assessment, Chinese Research Academy of Environmental  
14 Sciences, Beijing, 100012, China

15 <sup>6</sup> Low-Carbon and Climate Impact Research Centre, City University of Hong Kong, Hong Kong, China

16  
17 *Correspondence to:* Chak K. Chan ([chak.k.chan@cityu.edu.hk](mailto:chak.k.chan@cityu.edu.hk))

18 **Abstract.** Incense burning is a common religious activity that emits abundant gaseous and particulate pollutants into the  
19 atmosphere. During their atmospheric lifetime, these gases and particles are subjected to (photo-)oxidation, leading to the  
20 formation of secondary pollutants. We examined the oxidation of incense burning plumes under O<sub>3</sub> exposure and dark  
21 condition using an oxidation flow reactor connected to a single particle aerosol mass spectrometer (SPAMS). Nitrate formation  
22 was observed in incense burning particles, mainly attributable to the ozonolysis of nitrogen-containing organic compounds.  
23 With UV on, nitrate formation was significantly enhanced, likely due to HNO<sub>3</sub>/HNO<sub>2</sub>/NO<sub>x</sub> uptake triggered by OH chemistry,  
24 which is more effective than ozone oxidation. The extent of nitrate formation is insensitive to O<sub>3</sub> and OH exposure, which can  
25 be explained by the diffusion limitation on interfacial uptake. The OH-aged particles are more oxygenated and functionalized  
26 than O<sub>3</sub>-aged particles. Oxalate and malonate, two typical secondary organic aerosols (SOA), were found in OH-aged particles.  
27 Our work reveals that nitrate, accompanied by SOA, can rapidly form in incense-burning particles upon photochemical  
28 oxidation in the atmosphere, which could deepen our understanding of air pollution caused by religious activities.

## 29 1 Introduction

30 Incense burning is a common religious ritual, especially in Asian and African communities (Ye et al., 2016; Khezri et al.,  
31 2015; Sidibe et al., 2022), with a massive amount of particles emitted (Lyu et al., 2021; See and Balasubramanian, 2011). The  
32 PM<sub>2.5</sub> concentration at a shrine area reached 6-8 times higher than usual during the Chinese New Year in Chiang Mai, Thailand,  
33 mainly due to incense burning (Bootdee et al., 2016). The particle emission factor (i.e., the mass ratio of the emitted particles



34 to the total material burnt) from incense burning could be up to 10 times higher than those from burning of various types of  
35 biomasses such as rice straw (Akagi et al., 2011; See and Balasubramanian, 2011; Goel et al., 2020).

36 Previous research mainly focused on the chemical compositions and potential health impacts of fresh incense particles (Li et  
37 al., 2012; Wang et al., 2006; Chuang et al., 2011; Lee and Wang, 2004). However, it was rarely considered that fresh particles  
38 would also be exposed to other atmospheric pollutants and light, which could initiate chemical reactions. The formation of  
39 secondary particulate pollutants could take place during the atmospheric aging of particles (Hodshire et al., 2019; Kumar et  
40 al., 2018; Rudich et al., 2007). For example, our recent work reveals rapid sulfate formation in fresh incense burning particles  
41 upon SO<sub>2</sub> exposure in the dark, and it can be accelerated under light (Liang et al., 2022a). Sulfate formation in incense burning  
42 particles under dark and light was mainly attributed to gaseous oxidants and particulate photosensitizers, respectively.

43 Ozone and OH radicals are two of the most common oxidants in the atmosphere, contributing to secondary inorganic and  
44 organic aerosol formation (Volkamer et al., 2006; Kroll et al., 2006; Chen et al., 2011; Liu et al., 2019; Liu et al., 2018).  
45 Incense burning plume has been reported to contain various volatile organic compounds (VOCs) and NO<sub>x</sub> (Lee and Wang,  
46 2004; Ho and Yu, 2002), in addition to particulate pollutants. Their interactions with ozone and OH radicals may lead to  
47 secondary aerosol formation. For instance, oxidations of NO<sub>x</sub> by ozone and OH radicals were considered primary sources of  
48 particulate nitrate (Seinfeld and Pandis, 2008; Liang et al., 2021; Gen et al., 2022). Nevertheless, there is still a lack of  
49 understanding of the secondary aerosol formation in incense burning particles upon atmospheric aging of the plume, which  
50 could potentially worsen air quality, especially near areas of intense religious activities.

51 This study examines the secondary aerosol formation in fresh incense burning particles under ozone and OH exposure using a  
52 Gothenburg Potential Aerosol Mass (Go: PAM) flow reactor. We first characterized single fresh incense burning particles,  
53 followed by aged particles, with a single-particle aerosol mass spectrometer (SPAMS). Control experiments were performed  
54 to get insight into the possible secondary aerosol formation pathways and their significance. Then, we discussed nitrate  
55 formation as a function of particle size, ozone, and OH exposure. The fragmentation severely hinders the characterization of  
56 secondary organic aerosol (SOA). Nevertheless, -89[C<sub>2</sub>HO<sub>4</sub>] (oxalate) and -103[C<sub>3</sub>H<sub>3</sub>O<sub>4</sub>] (malonate), two commonly  
57 considered SOA (Cheng et al., 2017; Sullivan and Prather, 2007), were found.

58

## 59 **2 Experimental**

### 60 **2.1 Aging of incense-burning particles**

61 The schematic of the experimental set-up can be found in Figure S1 and our previous publication (Liang et al., 2022a). In brief,  
62 we burnt an incense stick in a 20 L glass burning bottle. The burning was rapidly converted from flaming to smoldering after  
63 ignition. A two-stage system diluted the emissions with an overall dilution of around 1600. Compressed air (~0.1 L min<sup>-1</sup>) was



64 used to introduce the diluted incense burning particles to the PAM reactor equipped with two UVC light tubes (30W, Philips  
65 TUV,  $\lambda_{\text{max}} = 254\text{nm}$ ). In the control experiments, a charcoal absorber or HEPA filter was used to remove the gaseous  
66 pollutants or particles prior to the introduction to the PAM. The removal efficiency of NO<sub>x</sub>, VOCs, and particles are ~85%,  
67 ~90%, and ~100%, respectively. A controlled dry-wet mixed carrier flow of compressed air (~4 L min<sup>-1</sup>) and a flow of O<sub>3</sub>  
68 (~0.1 L min<sup>-1</sup>) generated by passing O<sub>2</sub> (99.995%, Linde) to an O<sub>3</sub> generator (Model 610, Jelight Company Inc, USA) were  
69 introduced into the PAM. [O<sub>3</sub>] ranged from 300 to 1500 ppb, equivalent to an atmospheric ozone exposure of 10-50 min,  
70 assuming ambient concentration of 60 ppb (Xia et al., 2021). The relative humidity (RH) at the exit of the PAM was monitored  
71 by an RH sensor (M170, Vaisala, Finland). All the experiments were conducted at 80% RH. The exhaust of the PAM was  
72 characterized by an O<sub>3</sub> analyzer (106L, 2B technology, USA), a water-based condensation particle counter (WCPC, Aerosol  
73 dynamics Inc, USA), and a SPAMS (Hexin Analytical Instrument Co., Ltd, China). The particles were passed through a  
74 diffusion dryer before entering the PAM, to reduce the matrix effects from water (Neubauer et al., 1998). We also collected  
75 particles on 47 mm quartz filters (PALL, USA) at the exhaust of the PAM reactor for offline analysis. The number of particles  
76 collected on the filters was estimated by the total WCPC counts during the sampling period. The filter sample was extracted  
77 by deionized (DI) water for analyzing water-soluble ions (e.g., nitrate, formate, potassium) by Ion chromatography (IC) using  
78 the same protocol reported in our previous work (Liang et al., 2022a).

79  
80 We studied the aging of the particles under 'UV', 'O<sub>3</sub> and dark', and 'O<sub>3</sub> and UV' in the PAM. Since UV at 254 nm is expected  
81 to photolyze O<sub>3</sub> to form OH radicals in the presence of water vapor, we named these aged particles UV-aged, O<sub>3</sub>-aged, and  
82 OH-aged, respectively. Although 254 nm is not atmospherically relevant, UV-aged particles are used as a reference in the  
83 discussions of the properties of OH-aged particles. The OH exposure, equivalent to the product of gas-phase OH concentration  
84 and residence time, was determined by introducing a stream of SO<sub>2</sub> to the PAM for consuming OH radicals and monitoring  
85 the [SO<sub>2</sub>] decay, following a well-established approach in the literature (Kang et al., 2007). [SO<sub>2</sub>] was almost constant under  
86 UV on but without O<sub>3</sub>, suggesting that the photochemistry of incense plume does not affect our estimation of OH exposure.  
87 The upper limit of OH exposure used in this study varied from  $1 \times 10^{10}$  to  $5 \times 10^{10}$  molecules cm<sup>-3</sup> s, equivalent to 2~10 hours  
88 of photochemical aging, assuming an ambient OH concentration of  $1.5 \times 10^6$  molecules cm<sup>-3</sup> (Mao et al., 2009).

89

## 90 2.2 SPAMS analysis

91 A detailed description of the SPAMS can be found in Li et al (Li et al., 2011). After the particle flow exits the PAM reactor,  
92 it first passes a PM<sub>2.5</sub> cyclone to avoid clogging before entering the SPAMS through a 0.1 mm critical orifice at 80 mL min<sup>-1</sup>  
93 flow. Particles achieved a terminal velocity in the supersonic expansion airflow and were detected and aerodynamically sized  
94 by two continuous diode Nd: YAG laser beams (532 nm). They were then ionized by a pulsed Nd: YAG laser (266 nm)  
95 triggered based on the velocity of a specific particle. The positive and negative ions produced were detected according to the  
96 different mass-to-charge ratios (m/z). The energy of the ionization laser was kept at ~0.6 mJ (Cheng et al., 2017). Spectra of



97 more than 3000 individual particles collected for ~15 min were used for further analysis for each experiment. The instrument  
98 was routinely calibrated with polystyrene latex spheres of 0.2-2.5  $\mu\text{m}$  diameter (Nanosphere Size Standards, Duke Scientific  
99 Corp., Palo Alto). An adaptive resonance theory method (ART-2a) based on MATLAB was used to categorize the incense  
100 particles of similar SPAMS spectral characteristics into different particle groups (Phares et al., 2001). In the ART-2a analysis,  
101 we used a vigilance factor of 0.85, a widely adopted high level (Xu et al., 2018; Wang et al., 2019), and more than 98% of the  
102 particles were analyzed.

103

## 104 **3 Results and discussions**

### 105 **3.1 Single-particle characteristics of incense burning particles**

106 The relative peak area (RPA), defined as the peak area of a specific peak divided by the total positive or negative mass spectral  
107 peak area, can reflect the relative abundance of particulate components (Liang et al., 2022a). The average spectra of the incense  
108 burning particles (Figure 1a) are similar to our previous work on incense burning at 50% RH (Liang et al., 2022b). +39[K]  
109 dominates the positive spectra, and organic nitrogen (ON) peaks (i.e., -26[CN] and -42[CNO]) from nitrogen-containing  
110 organics (NOC) dominate the negative spectra (Zhang et al., 2020; Zhai et al., 2015; Zhang et al., 2021). These features are  
111 also found in biomass burning particles (Bi et al., 2011; Peng et al., 2019; Luo et al., 2020).

112

113 ART-2a categorizes fresh incense burning particles into K-ON, K-ONEC, K-Cl, and OC-ON. Briefly, the "K" and "OC" before  
114 the hyphen indicate the characteristics of the positive spectra, while "ON", "ONEC" and "Cl" after the hyphen indicate the  
115 features of the negative spectra. "K-" particles contain a dominant +39 peak and a small +41 peak attributed to isotopic  
116 potassium (Bi et al., 2011). On the other hand, the "OC-" particles are rich in typical organic fragments such as +27[C<sub>2</sub>H<sub>3</sub>]  
117 (Cheng et al., 2017). According to the negative spectra, "-ON" particles have dominant ON signals. "-ONEC" particles have  
118 elemental carbon (EC) peaks of -12n[C<sub>n</sub><sup>-</sup>], with intensities comparable to typical ON peaks (Zhou et al., 2020). "-Cl" particles  
119 have prominent Cl<sup>-</sup> (m/z=-35, -37(isotopic)) and KCl<sub>2</sub><sup>-</sup> (m/z=-109, -111(isotopic)) peaks (Bi et al., 2011). The average spectra  
120 of each category can be found in Figure S2. There are slightly fewer K-ON particles and more K-ONEC particles observed at  
121 80% RH (this work) than at 50% RH in Liang et al (Liang et al., 2022b), probably due to the lower organic concentrations at  
122 higher RH to limit particle-phase partitioning of volatile organic compounds (Donaldson and Vaida, 2006; Mcfall et al., 2020;  
123 Chan and Chan, 2011; Chan et al., 2010). Overall, the number fraction (NF) of each category is similar to our previous work,  
124 with a descending order of K-ON (47.3±5.2%) >> OC-ON (25.7±4.7%) ≈ K-ONEC (20.2±2.8%) > K-Cl (5.1±1.1%) (Figure  
125 1c), reflecting the fresh incense burning particles are organic-rich (Li et al., 2012; Zhang et al., 2022a).

126



### 127 3.2 Ozonolysis of the incense burning particles

128 Figure 1a also shows the average spectra of aged incense burning particles under 800 ppb O<sub>3</sub>. Qualitatively, the major peaks  
129 are similar to those in fresh incense burning particles, except for the rise of -62[NO<sub>3</sub><sup>-</sup>] and -46[NO<sub>2</sub><sup>-</sup>], which indicates the  
130 formation of nitrate and probably nitrite. The formation of organo-nitrate is not considered significant due to the decreased -  
131 26[CN] and -42[CNO].

132

133 To compare the changes in the organic signals, we first excluded all inorganics and EC peaks (Table S1). Control experiments  
134 atomizing KNO<sub>3</sub> solution (as K<sup>+</sup> is the main inorganic cation found in incense burning particles) showed the RPA ratio of -  
135 16[O] to nitrate peaks is (6 ± 1.7) % due to fragmentation. Sulfate shows negligible fragment under our experimental conditions  
136 (Liang et al., 2022a). Thus, we subtracted the RPA of -16[O] by 6% RPA of nitrate. Then, we recalculated the relative peak  
137 area (RPA) of the organic peaks only. Figure 1b shows the differences in the spectra of the aged and fresh particles. The  
138 positive difference spectra show an RPA increase in the hydrocarbon +37[C<sub>3</sub>H] but an RPA decrease in +51[C<sub>4</sub>H<sub>3</sub>] (Dall'osto  
139 et al., 2013). Besides, the increase of +28[CO], +42[C<sub>2</sub>H<sub>2</sub>O], and +43[C<sub>2</sub>H<sub>3</sub>O] indicates the formation of oxidized organics in  
140 the particles during ozonolysis. The negative difference spectra show a decrease in ON peaks, possibly due to the destruction  
141 of C-N bonds under ozonolysis, and an increase of -45[CHO<sub>2</sub>] formate peak.

142

143 NO<sub>2</sub> emitted by incense burning may hydrolyze in the incense burning particles to form nitrite and nitrate (2NO<sub>2</sub> + H<sub>2</sub>O =>  
144 HNO<sub>2</sub> + HNO<sub>3</sub>) (Finlayson-Pitts et al., 2003; Ramazan et al., 2006). The uptake of NO<sub>2</sub> is slow in deionized water ( $\gamma \approx 10^{-7}$ ),  
145 but it could be significantly promoted by chloride ( $\gamma \approx 10^{-3}$  in 1mM NaCl) (Enami et al., 2009; Yabushita et al., 2009), which  
146 is found as major inorganic anion in the incense burning particles. In addition, the reaction between NO<sub>2</sub> and O<sub>3</sub> produces NO<sub>3</sub>  
147 radicals, which could react with organics to form organo-nitrate (Ng et al., 2017). However, control experiments using a  
148 charcoal absorber to remove NO<sub>x</sub> only show ~20% decrease in RPA of total nitrate in O<sub>3</sub> aged particles (Figure S3), indicating  
149 that NO<sub>2</sub> hydrolysis and nitration may not be the main contributor to the nitrate formation. We categorized the O<sub>3</sub>-aged particles  
150 into 7 groups of K-ON, K-ONEC, K-ONN, K-N, K-Cl, OC-N, and OC-ON particles by ART-2a. The definitions of K-, OC-,  
151 -ON, -ONEC, -Cl are the same as before. -N particles show prominent nitrate peaks (-46[NO<sub>2</sub>] and -62[NO<sub>3</sub>]) in the negative  
152 spectra, while -ONN particles show comparable ON peaks and nitrate peaks (Figure S2). The NF of different categories  
153 descends in the order of K-ON (29.0±0.7%) ≈ K-ONEC (22.8±1.8%) ≈ OC-N (21.9±1.0%) > K-ONN (11.2±0.9%) > OC-ON  
154 (7.6±1.7%) > K-Cl (3.9±0.4%) > K-N (2.5±0.5%) (Figure 1c). Interestingly, the K-ONEC and K-Cl NFs are similar before  
155 and after aging, whereas the K-ON NF decreased, and the decrease is comparable to the sum of the K-ONN and K-N NF  
156 increases. OC-ON was the only fresh OC- particle type, but OC-N was dominant after aging. A control experiment with a  
157 HEPA filter before the PAM showed no detectable particles by SPAMS. Thus, we assume the total SPAMS-detectable particle  
158 number was constant before and after aging, and O<sub>3</sub>-aging may have preferentially converted some -ON type particles to  
159 nitrate-containing particles (i.e., -ONN, -N). Besides, O<sub>3</sub>-aged particles have lower ON (i.e., the sum of -26[CN] and -



160 42[CNO]) absolute peak area (APA) and higher total nitrate APA (i.e., -46[NO<sub>2</sub>] and -62[NO<sub>3</sub>]), than fresh particles (Figure  
161 S4). We considered -46[NO<sub>2</sub>] mainly as a nitrate fragment but not nitrite since the IC-measured [NO<sub>2</sub><sup>-</sup>]/[NO<sub>3</sub><sup>-</sup>] in the water-  
162 extract of collected particles was very low (~0.01) (Figure S5). We used APA here because it reflects the total abundance of  
163 ions and would not affect the analysis of other ions (Spencer and Prather, 2006). The formation of nitrate would increase the  
164 total peak area and decrease the RPA of other peaks, even the APA of others kept constant. Figure S6 also shows a positive  
165 correlation between the total nitrate RPA and formate RPA in the aged particles. Based on offline IC analysis, the water-extract  
166 of O<sub>3</sub>-aged particles has higher [Formate]/[K<sup>+</sup>] and [NO<sub>3</sub><sup>-</sup>]/[K<sup>+</sup>] in than fresh particles (Figure S7), assuming that K<sup>+</sup> is not  
167 reactive and used as an internal standard (Figure S8). Taking these altogether, nitrate and formate likely formed together,  
168 preferentially on K-ON and OC-ON particles. Ozonolysis of NOC has been reported to generate nitrate and formate (Sharma  
169 and Graham, 2010; Yao et al., 2020).

170

### 171 3.3 Photochemical oxidation of incense burning particles

172 With UV (254nm) on, the 800 ppb O<sub>3</sub> was partly photolyzed to generate OH radicals in the presence of water vapor, resulting  
173 in an OH exposure of ~3× 10<sup>10</sup> molecules cm<sup>-3</sup> s, equivalent to a photochemical age of ~5 h. We will use xx ppb O<sub>3</sub> (initial  
174 concentration) +UV, instead of OH exposure, to describe OH aging. The average spectra of OH-aged particles are generally  
175 similar to that of O<sub>3</sub>-aged particles, with potassium and nitrate peaks dominating the positive and negative spectra, respectively  
176 (Figure 1a). However, the RPA of -46[NO<sub>2</sub>] and -62[NO<sub>3</sub>] were 0.2 and 0.4, around 2 times higher than O<sub>3</sub>-aged particles,  
177 likely indicating more nitrate formation. As will be discussed later, photochemistry triggered by light-absorbing compounds  
178 such as photosensitizers and Fe salts is a possible source of nitrate formation in OH-aged particles.<sup>51-53</sup> However, its  
179 contribution is considered minor compared with OH chemistry since UV-aged particles only show a total nitrate RPA of 0.05,  
180 much lower than that of OH-aged particles (~ 0.7, will be discussed later). Control experiments using a charcoal absorber to  
181 remove the NO<sub>x</sub> significantly reduced the RPA of total nitrate by ~75% (Figure S3). These suggest that OH chemistry  
182 involving NO<sub>x</sub> dominated the particulate nitrate formation under OH exposure. Under 800 ppb O<sub>3</sub> and UV, the ~90% reduction  
183 of [NO<sub>x</sub>] with a simultaneous increase in total nitrate peaks under UV suggests the oxidation of NO<sub>x</sub> by OH radicals to form  
184 HNO<sub>2</sub> and HNO<sub>3</sub>, which can be uptake by the particles afterward (Finlayson-Pitts and Pitts Jr, 1999). Reactive uptake of NO<sub>x</sub>  
185 initiated by OH chemistry cannot be excluded.

186

187 Similar to the O<sub>3</sub>-aged particles, OH-aged particles show decreases in ON and other organic peaks (+38[C<sub>3</sub>H<sub>2</sub>], +50[C<sub>4</sub>H<sub>2</sub>],  
188 and +51[C<sub>4</sub>H<sub>3</sub>]) in the difference organic averaged spectra (Silva and Prather, 2000), likely due to oxidative consumption by  
189 OH radicals (Figure 1b). The ON peaks decrease in OH-aged particles was more significant than in O<sub>3</sub>-aged particles, whereas  
190 the increase in formate peak is less obvious. These indicate that NOCs can also be effectively degraded via OH oxidation.  
191 Using the commonly used general markers of oxidized/aged organics in single-particle mass spectrometric studies of -16[O],  
192 -17[OH], +42[C<sub>2</sub>H<sub>2</sub>O], and +43[C<sub>2</sub>H<sub>3</sub>O] as examples (Taiwo et al., 2014; Denkenberger et al., 2007; Qin and Prather, 2006),





193 the RPA increase in OH-aged particles are 18, 10, 3, and 17 times higher than in O<sub>3</sub>-aged particles. This suggests that OH  
194 aging produced more oxidized and functionalized products than O<sub>3</sub> aging. The difference average organic spectra of UV-aged  
195 particles almost showed no noticeable peaks, indicating that the chemistry initiated by particulate photoactive compounds may  
196 not be essential to the transformation of the organics (Figure S9).

197

198 The OH-aged particles can be categorized into K-ONN, K-N, and OC-N, and they generally have more intense nitrate peaks  
199 than O<sub>3</sub>-aged particles. Still, "-ONN" particles have comparable ON and nitrate peaks, and "-N" particles have dominant nitrate  
200 peaks in the negative spectra (Figure S2). The NF descends in the order of OC-N (35.7±7.2%) ≈ K-N (35.5±4.2%) > K-ONN  
201 (25.7±2.1%) (Figure 1c). Notably, the NF of OC- particles of OH-aged particles is 50% larger than the fresh particles, likely  
202 due to the formation of additional particulate organics. We could not identify any preferential nitrate formation in specific  
203 particle types since most of the particles have high RPA of nitrate.

204

### 205 3.4 The formation of secondary nitrate

206 Figure 2a shows the RPA of nitrate peaks under UV and different exposure of O<sub>3</sub> and OH. Since fresh particles also have high  
207 NF of total nitrate, NF cannot accurately depict the effectiveness of nitrate formation. Fresh incense burning particles exhibit  
208 very low RPA of total nitrate, whereas exposure to O<sub>3</sub> increases the RPA from almost 0 to around 0.2, irrespective of the [O<sub>3</sub>].  
209 Only a slight increase (~0.02) in total nitrate RPA was observed for UV-aged particles. However, with both O<sub>3</sub> and UV on,  
210 the RPAs of total nitrate further increased to above 0.7, which is also independent of the initial [O<sub>3</sub>]. Consistent with the  
211 average spectra shown before, nitrate formation due to OH oxidation is likely more efficient than that by ozonolysis. Under  
212 both O<sub>3</sub> and OH exposure, the summed APA of nitrate peaks increased as particle size increased, suggesting possibly a larger  
213 total amount of nitrate formed in larger particles (Figure 2b, d). However, the RPA shows an opposite trend, which can be  
214 interpreted as lower nitrate concentration in larger particles. Larger particles have larger surfaces but smaller surface-to-volume  
215 ratios, which lead to a larger absolute amount of nitrate formed but a lower relative concentration of particulate nitrate (Figure  
216 2c, e). Under O<sub>3</sub>+UV, it is also possible that comparable HNO<sub>3</sub> was generated under excess [OH] and contributed to the similar  
217 total nitrate RPA since the [NO<sub>x</sub>] reductions under different OH exposure are similarly high (Figure S10). The insensitivity of  
218 nitrate formation to O<sub>3</sub> and OH exposure can be potentially explained by the diffusion limitation of interfacial uptake due to  
219 the poor hygroscopicity of fresh incense burning particles (Li and Hopke, 1993; Zaveri et al., 2018; Slade and Knopf, 2014;  
220 Liang et al., 2022a).

221

### 222 3.5 The Potential formation of SOA

223 Oxalate and malonate are two major dicarboxylates in atmospheric particles and are considered SOA (Yao et al., 2002). They  
224 have been widely studied using single-particle mass spectrometry with well-validated detection efficiency, without severe



225 complications in mass spectra due to fragmentations (Cheng et al., 2017; Sullivan and Prather, 2007). Figure 3a shows the NF  
226 ratio (aged particles to fresh particles) of oxalate and malonate. We used the NF ratio rather than the APA or RPA, to avoid  
227 large uncertainties in organic abundance due to the much weaker peaks of organics in the spectra.

228

229 NFs of malonate and oxalate increase with OH exposure, to 30 and 9 folds, respectively, at 1500 ppb O<sub>3</sub> and UV. This trend  
230 is opposite to the independence of nitrate formation on OH exposure, probably because their formations are relatively slower.  
231 These are lower estimates due to the possible degradation by photolysis of Fe-decarboxylate complexes to CO<sub>2</sub> (Gen et al.,  
232 2021). In contrast, no oxalate and malonate were observed during ozonolysis, irrespective of [O<sub>3</sub>]. Furthermore, UV-aged  
233 particles did not show an NF increase of both, indicating that the oxalate and malonate formation were mainly due to OH  
234 radicals, rather than oxidants from particulate photoactive compounds or ozone. The control experiment with a charcoal  
235 absorber shows around 60% and 70% NF reduction of oxalate and malonate, suggesting that the precursors are mainly in the  
236 gas phase (Figure S11). The size distribution of oxalate and malonate containing particles skewed towards the larger sizes,  
237 supporting their nature of secondary formation (i.e., oxidized gaseous precursors were added to the particles that cause size  
238 increase, Figure S12). Figure 3b shows the NF of oxalate and malonate in different categories of the particles. The particles in  
239 the replicated experiments under the same OH exposure were combined to compensate for the low particle concentrations.  
240 The error bars show one standard deviation among different OH exposures. In descending order, the NF of oxalate and  
241 malonate was K-N > K-ONN > OC-N. The mass hygroscopic grow factor (i.e., the mass ratio of wet particles to dry particles)  
242 of inorganic potassium salts KNO<sub>3</sub> and KCl at 80% RH are around 1.6 and 2.2 based on AIOMFAC model predictions (Text  
243 S1, <https://aiomfac.lab.mcgill.ca/about.html> (Zuend et al., 2008)), much higher than that in the water extract of biomass  
244 burning particles (1.1-1.4, including both lab-generated and ambient collected) (Rissler et al., 2006; Carrico et al., 2008; Chan  
245 et al., 2005), as well as fresh incense burning particles (around 1) (Liang et al., 2022b), which are organic-rich. The likely  
246 higher fraction of hygroscopic inorganic of inorganic fraction allows K-N and K-ONN to retain more liquid water to dissolve  
247 gaseous SOA precursors for oxalate and malonate formation. The difference of oxalate and malonate NF is statistically  
248 significantly different between K-N and OC-N (i.e., P < 0.05 in ANOVA test). There are many other changes in the NF of  
249 organic fragments, which suggest the oxidation of primary organics and the formation of SOA. However, further analysis was  
250 limited by the lack of molecular information after severe fragmentation. The major spectral evolution and possible peak  
251 attribution can be found in Text S2.

252

#### 253 4 Conclusions

254 In this work, we report single-particle characteristics of incense burning particles upon ozonolysis and photochemical  
255 oxidation. Nitrate formation initiated by O<sub>3</sub> is generally considered to involve the so-called N<sub>2</sub>O<sub>5</sub> pathway, in which oxidation  
256 of NO<sub>x</sub> forms NO<sub>3</sub> radical and then N<sub>2</sub>O<sub>5</sub>, which hydrolyzes to form particulate nitrate (Zhao et al., 2021; Xiao et al., 2020).  
257 In our study, nitrate formation was found, as indicated by the increase of total nitrate RPA from near 0 to around 0.2, upon O<sub>3</sub>





258 exposure. We propose that ozonolysis of NOCs may be a potential pathway for nitrate formation, in addition to the  $N_2O_5$   
259 pathway. With UV on, ozone was photolyzed to form OH radicals, and we observed a significant increase in total nitrate RPA  
260 to above 0.7 at 300 ppb  $O_3$  or above. Nitrate formation in OH-aged particles is more prominent than in  $O_3$ -aged particles and  
261 is attributed to multiphase OH oxidation involving  $NO_x$ , such as  $HNO_3/HNO_2/NO_x$  uptake (Chen et al., 2020; Lu et al., 2019).  
262 At 300 ppb  $O_3$  and UV in this study, the equivalent OH and  $O_3$  exposure time of the incense particles is estimated to be ~2 h  
263 and ~10 min, respectively, assuming daytime OH and  $O_3$  concentration of  $1.5 \times 10^6$  molecules  $cm^{-3}$  and 60 ppb (Xia et al.,  
264 2021; Mao et al., 2009). Despite the differences in the estimated exposure time for OH and  $O_3$ , nitrate formation in incense  
265 particles under sunlight can be efficient.

266

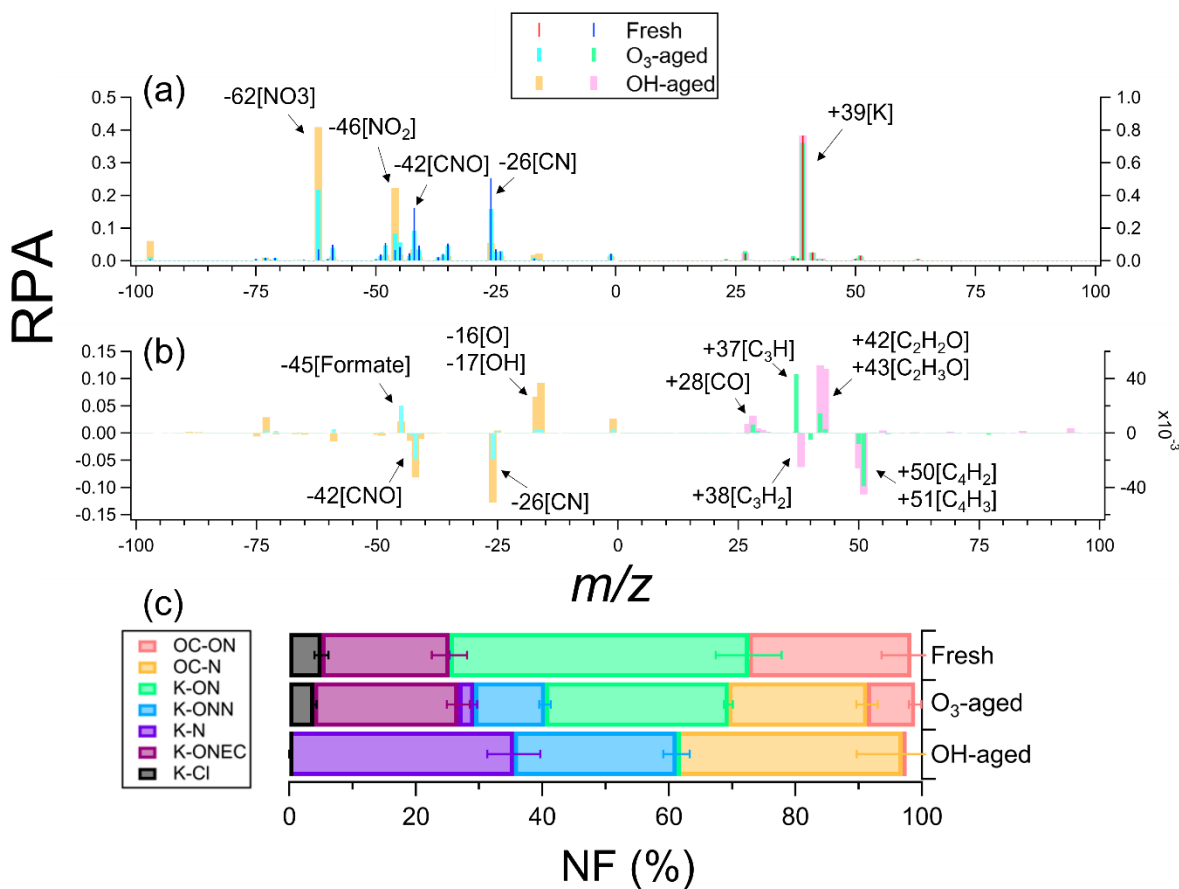
267 We also observed various changes in organics peaks, though less apparent than nitrate in the average spectra. Overall,  
268 oxygenated fragments like  $+42[C_2H_2O]$  increase, which indicates functionalization of the organics upon oxidation. The  
269 increase of such oxygenated fragments is more significant in OH-aged than  $O_3$ -aged particles.  $-26[CN]$  and  $-42[CN O]$   
270 attributed to NOC decreased under  $O_3$  and OH exposure. Apparent formate formation was observed in  $O_3$ -aged particles, likely  
271 from the degradation of NOC. Production of formate in OH-aged particles was less significant than that in  $O_3$ -aged particles,  
272 attributed to the photolysis of  $O_3$ . Oxalate and malonate were observed in OH-aged particles but not in  $O_3$ -aged particles, and  
273 the NFs increased with OH exposure. Furthermore, oxalate and malonate preferentially formed on K-N particles, followed by  
274 K-ONN and then OC-N, indicating a potentially crucial role of aerosol liquid water in SOA formation.

275

276 Though the molecular characterization of SOA is beyond the focus of this work, the formation of oxalate and malonate shed  
277 light on the SOA formation upon photochemical oxidation of the incense burning plumes. Formate and dicarboxylates are  
278 important hygroscopic organics in atmospheric particles, which can potentially act as cloud condensation nuclei (Yao et al.,  
279 2002; Peng and Chan, 2001). Incense burning particles were often used as biomass burning particle surrogates (Li et al., 2012;  
280 Schurman et al., 2017; Zhang et al., 2014; Kuwata and Lee, 2017), due to their similar physicochemical properties and overall  
281 composition (Li et al., 2012; Zhang et al., 2022b). Our work sheds light on the secondary aerosol formation in biomass burning  
282 particles upon exposure of atmospheric oxidants, despite that the detailed composition of incense burning plume may be  
283 different from biomass burning plume because of the manufacturing process of incense sticks. For instance, incense burning  
284 sticks may contain additives such as adhesives beyond biomass constituents (Lin et al., 2007). Future works are encouraged to  
285 explore the formation mechanism and kinetics of secondary pollutants in the incense burning and biomass burning particles.  
286 Due to the short residence time in a PAM reactor, assumption in the interchangeability of oxidant concentration and reaction  
287 time in estimating total exposure was made. However, Chu et al. (2019) challenged such interchangeability in ozonolysis  
288 reaction of linoleic acid (Chu et al., 2019). Aging at ambient concentrations of oxidants should also be investigated.

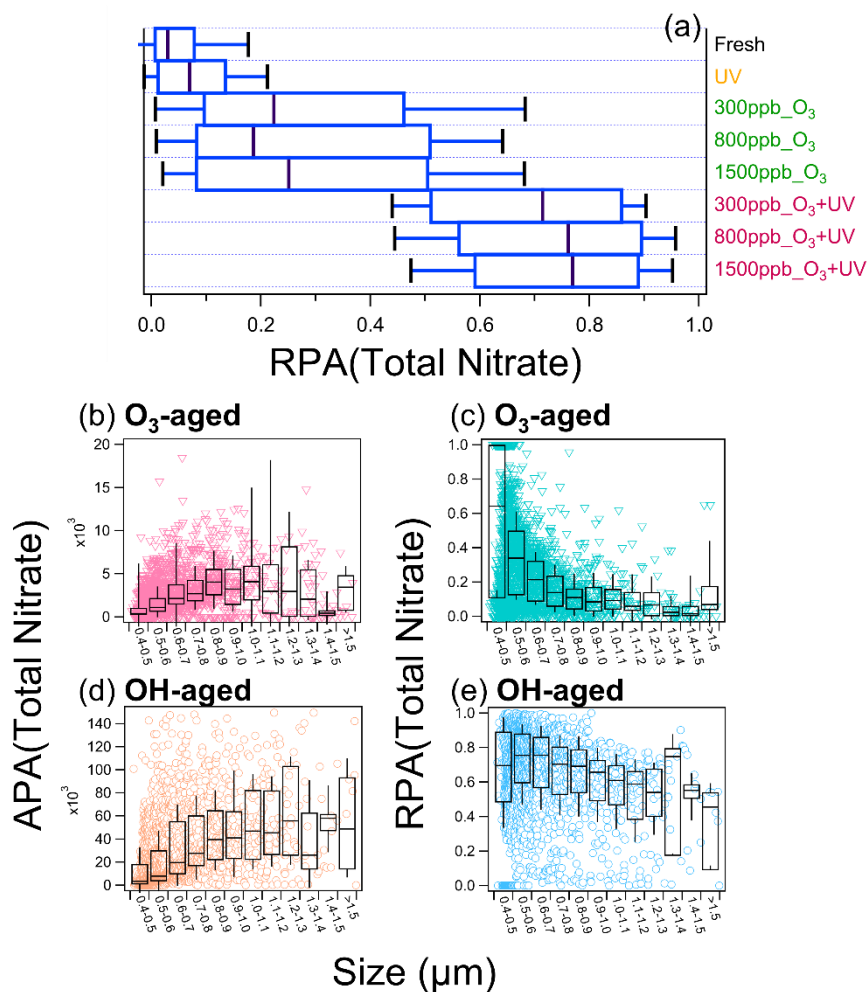
289

290



291  
 292 **Figure 1.** (a) The average spectra of fresh and aged incense burning particles at 800 ppb O<sub>3</sub>(+UV); (b) The difference (aged  
 293 minus fresh) of the average organic spectra of incense burning particles at 800 ppb O<sub>3</sub>(+UV). The left axis and right axis are  
 294 for negative spectra and positive spectra, respectively. (c) Number fraction of different categories in fresh, O<sub>3</sub>-aged, and OH-  
 295 aged particles.

296



297

298 **Figure 2.** (a) The whisker-box plot of total nitrate RPA of fresh and aged particles. The whisker-box plots of (b, d) APA and  
299 (c, e) RPA of total nitrate in O<sub>3</sub>- and OH-aged particles as a function of size (unit: μm) of particles aged at 1500 ppb O<sub>3</sub> (+  
300 UV). The medians are shown as the lines in the boxes, and the error bars represent one standard deviation.

301

302

303

304

305

306

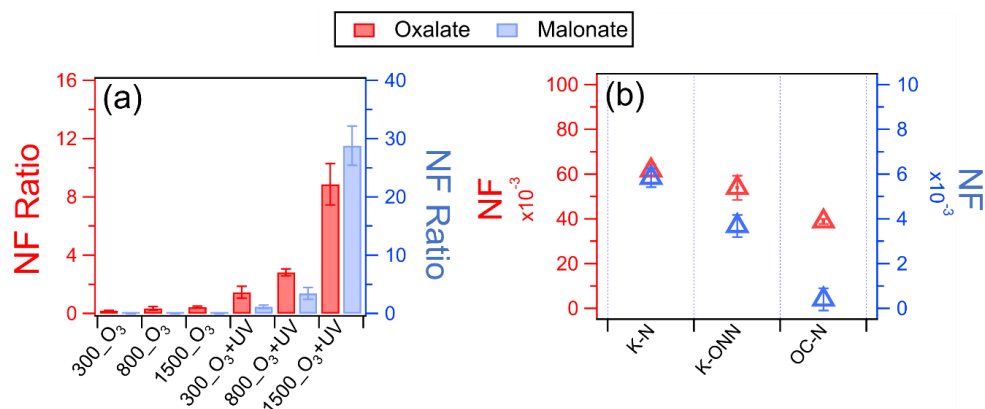
307

308



309

310



311

312 **Figure 3.** (a) The NF ratios of oxalate and malonate under different conditions. 300\_O<sub>3</sub> denotes aging at 300 ppb O<sub>3</sub>; (b) The  
313 NF of oxalate (left axis) and malonate (right axis) in different categories of aged particles.

314

315

316 *Data availability.* The supplement provides additional figures and tables.

317

318 *Competing interests.* The contact author has declared that neither they nor their co-authors have any competing interests.

319 Financial support.

320

321 *Acknowledgment.* We gratefully acknowledge the support from the Key-Area Research and Development Program of  
322 Guangdong Province (2020B1111360001), the Hong Kong Research Grants Council (No.11304121, R1016-20F), the National  
323 Natural Science Foundation of China (No. 42275104, 41905122).

324

## 325 References

326 ^Akagi, S. K., Yokelson, R. J., Wiedinmyer, C., Alvarado, M. J., Reid, J. S., Karl, T., Crouse, J. D., and Wennberg, P. O.:  
327 Emission factors for open and domestic biomass burning for use in atmospheric models, *Atmos. Chem. Phys.*, 11, 4039-4072,  
328 10.5194/acp-11-4039-2011, 2011.

329 ^Bi, X., Zhang, G., Li, L., Wang, X., Li, M., Sheng, G., Fu, J., and Zhou, Z.: Mixing state of biomass burning particles by  
330 single particle aerosol mass spectrometer in the urban area of PRD, China, *Atmospheric Environment*, 45, 3447-3453,  
331 <https://doi.org/10.1016/j.atmosenv.2011.03.034>, 2011.



- 332 ^Bootdee, S., Chantara, S., and Prapamontol, T.: Determination of PM<sub>2.5</sub> and polycyclic aromatic hydrocarbons from incense  
333 burning emission at shrine for health risk assessment, *Atmospheric Pollution Research*, 7, 680-689,  
334 <https://doi.org/10.1016/j.apr.2016.03.002>, 2016.
- 335 ^Carrico, C. M., Petters, M. D., Kreidenweis, S. M., Collett Jr., J. L., Engling, G., and Malm, W. C.: Aerosol hygroscopicity  
336 and cloud droplet activation of extracts of filters from biomass burning experiments, *Journal of Geophysical Research:*  
337 *Atmospheres*, 113, <https://doi.org/10.1029/2007JD009274>, 2008.
- 338 ^Chan, L. P. and Chan, C. K.: Enhanced Reactive Uptake of Nonanal by Acidic Aerosols in the Presence of Particle-Phase  
339 Organics, *Aerosol Science and Technology*, 45, 872-883, 10.1080/02786826.2011.567314, 2011.
- 340 ^Chan, L. P., Lee, A. K. Y., and Chan, C. K.: Gas-Particle Partitioning of Alcohol Vapors on Organic Aerosols, *Environmental*  
341 *Science & Technology*, 44, 257-262, 10.1021/es9018018, 2010.
- 342 ^Chan, M. N., Choi, M. Y., Ng, N. L., and Chan, C. K.: Hygroscopicity of Water-Soluble Organic Compounds in Atmospheric  
343 Aerosols: Amino Acids and Biomass Burning Derived Organic Species, *Environmental Science & Technology*, 39, 1555-  
344 1562, 10.1021/es049584l, 2005.
- 345 ^Chen, X., Hopke, P. K., and Carter, W. P.: Secondary organic aerosol from ozonolysis of biogenic volatile organic  
346 compounds: chamber studies of particle and reactive oxygen species formation, *Environmental science & technology*, 45, 276-  
347 282, 2011.
- 348 ^Chen, X., Wang, H., Lu, K., Li, C., Zhai, T., Tan, Z., Ma, X., Yang, X., Liu, Y., Chen, S., Dong, H., Li, X., Wu, Z., Hu, M.,  
349 Zeng, L., and Zhang, Y.: Field Determination of Nitrate Formation Pathway in Winter Beijing, *Environmental Science &*  
350 *Technology*, 54, 9243-9253, 10.1021/acs.est.0c00972, 2020.
- 351 ^Cheng, C., Li, M., Chan, C. K., Tong, H., Chen, C., Chen, D., Wu, D., Li, L., Wu, C., and Cheng, P.: Mixing state of oxalic  
352 acid containing particles in the rural area of Pearl River Delta, China: implications for the formation mechanism of oxalic acid,  
353 *Atmospheric Chemistry and Physics*, 17, 9519-9533, 2017.
- 354 ^Chu, Y., Cheng, T. F., Gen, M., Chan, C. K., Lee, A. K., and Chan, M. N.: Effect of ozone concentration and relative humidity  
355 on the heterogeneous oxidation of linoleic acid particles by ozone: an insight into the interchangeability of ozone concentration  
356 and time, *ACS Earth and Space Chemistry*, 3, 779-788, 2019.
- 357 ^Chuang, H.-C., Jones, T., Chen, Y., Bell, J., Wenger, J., and Bérubé, K.: Characterisation of airborne particles and associated  
358 organic components produced from incense burning, *Analytical and bioanalytical chemistry*, 401, 3095-3102, 2011.
- 359 ^Dall'Osto, M., Ovadnevaite, J., Ceburnis, D., Martin, D., Healy, R. M., O'Connor, I. P., Kourtchev, I., Sodeau, J. R., Wenger,  
360 J. C., and O'Dowd, C.: Characterization of urban aerosol in Cork city (Ireland) using aerosol mass spectrometry, *Atmospheric*  
361 *Chemistry and Physics*, 13, 4997-5015, 2013.
- 362 ^Denkenberger, K. A., Moffet, R. C., Holecek, J. C., Rebotier, T. P., and Prather, K. A.: Real-time, single-particle  
363 measurements of oligomers in aged ambient aerosol particles, *Environmental Science & Technology*, 41, 5439-5446, 2007.
- 364 ^Donaldson, D. J. and Vaida, V.: The Influence of Organic Films at the Air-Aqueous Boundary on Atmospheric Processes,  
365 *Chemical Reviews*, 106, 1445-1461, 10.1021/cr040367c, 2006.



- 366 ^Enami, S., Hoffmann, M. R., and Colussi, A.: Absorption of inhaled NO<sub>2</sub>, *The Journal of Physical Chemistry B*, 113, 7977-  
367 7981, 2009.
- 368 ^Finlayson-Pitts, B., Wingen, L., Sumner, A., Syomin, D., and Ramazan, K.: The heterogeneous hydrolysis of NO<sub>2</sub> in  
369 laboratory systems and in outdoor and indoor atmospheres: An integrated mechanism, *Physical Chemistry Chemical Physics*,  
370 5, 223-242, 2003.
- 371 ^Finlayson-Pitts, B. J. and Pitts Jr, J. N.: *Chemistry of the upper and lower atmosphere: theory, experiments, and applications*,  
372 Elsevier 1999.
- 373 ^Gen, M., Zhang, R., and Chan, C. K.: Nitrite/Nitrous Acid Generation from the Reaction of Nitrate and Fe(II) Promoted by  
374 Photolysis of Iron–Organic Complexes, *Environmental Science & Technology*, 55, 15715-15723, 10.1021/acs.est.1c05641,  
375 2021.
- 376 ^Gen, M., Liang, Z., Zhang, R., Go Mabato, B. R., and Chan, C. K.: Particulate nitrate photolysis in the atmosphere,  
377 *Environmental Science: Atmospheres*, 10.1039/D1EA00087J, 2022.
- 378 ^Goel, A., Mundra, R., and Ola, D.: Examination of Particle Characteristics and Quantification of Emission Factors for Smoke  
379 Generated from a Popular Indian Incense Burnt in an Experimental Chamber, in: *Indoor Environmental Quality*, Springer, 77-  
380 84, 2020.
- 381 ^Ho, S. S. H. and Yu, J. Z.: Concentrations of formaldehyde and other carbonyls in environments affected by incense burning,  
382 *Journal of Environmental Monitoring*, 4, 728-733, 10.1039/B200998F, 2002.
- 383 ^Hodshire, A. L., Akherati, A., Alvarado, M. J., Brown-Steiner, B., Jathar, S. H., Jimenez, J. L., Kreidenweis, S. M., Lonsdale,  
384 C. R., Onasch, T. B., and Ortega, A. M.: Aging effects on biomass burning aerosol mass and composition: A critical review  
385 of field and laboratory studies, *Environmental science & technology*, 53, 10007-10022, 2019.
- 386 ^Kang, E., Root, M., Toohey, D., and Brune, W.: Introducing the concept of potential aerosol mass (PAM), *Atmospheric*  
387 *Chemistry and Physics*, 7, 5727-5744, 2007.
- 388 ^Khezri, B., Chan, Y. Y., Tiong, L. Y. D., and Webster, R. D.: Annual air pollution caused by the Hungry Ghost Festival,  
389 *Environmental Science: Processes & Impacts*, 17, 1578-1586, 10.1039/C5EM00312A, 2015.
- 390 ^Kroll, J. H., Ng, N. L., Murphy, S. M., Flagan, R. C., and Seinfeld, J. H.: Secondary organic aerosol formation from isoprene  
391 photooxidation, *Environmental science & technology*, 40, 1869-1877, 2006.
- 392 ^Kumar, N. K., Corbin, J. C., Bruns, E. A., Massabó, D., Slowik, J. G., Drinovec, L., Močnik, G., Prati, P., Vlachou, A., and  
393 Baltensperger, U.: Production of particulate brown carbon during atmospheric aging of residential wood-burning emissions,  
394 *Atmospheric Chemistry and Physics*, 18, 17843-17861, 2018.
- 395 ^Kuwata, M. and Lee, W.-C.: 1-octanol-water partitioning as a classifier of water soluble organic matters: Implication for  
396 solubility distribution, *Aerosol Science and Technology*, 51, 602-613, 10.1080/02786826.2017.1283004, 2017.
- 397 ^Lee, S.-C. and Wang, B.: Characteristics of emissions of air pollutants from burning of incense in a large environmental  
398 chamber, *Atmospheric Environment*, 38, 941-951, <https://doi.org/10.1016/j.atmosenv.2003.11.002>, 2004.





- 399 ^Li, L., Huang, Z., Dong, J., Li, M., Gao, W., Nian, H., Fu, Z., Zhang, G., Bi, X., Cheng, P., and Zhou, Z.: Real time bipolar  
400 time-of-flight mass spectrometer for analyzing single aerosol particles, *International Journal of Mass Spectrometry*, 303, 118-  
401 124, <https://doi.org/10.1016/j.ijms.2011.01.017>, 2011.
- 402 ^Li, W. and Hopke, P. K.: Initial Size Distributions and Hygroscopicity of Indoor Combustion Aerosol Particles, *Aerosol*  
403 *Science and Technology*, 19, 305-316, 10.1080/02786829308959638, 1993.
- 404 ^Li, Y. J., Yeung, J. W. T., Leung, T. P. I., Lau, A. P. S., and Chan, C. K.: Characterization of Organic Particles from Incense  
405 Burning Using an Aerodyne High-Resolution Time-of-Flight Aerosol Mass Spectrometer, *Aerosol Science and Technology*,  
406 46, 654-665, 10.1080/02786826.2011.653017, 2012.
- 407 ^Liang, Z., Zhang, R., Gen, M., Chu, Y., and Chan, C. K.: Nitrate Photolysis in Mixed Sucrose–Nitrate–Sulfate Particles at  
408 Different Relative Humidities, *The Journal of Physical Chemistry A*, 125, 3739-3747, 10.1021/acs.jpca.1c00669, 2021.
- 409 ^Liang, Z., Zhou, L., Infante Cuevas, R. A., Li, X., Cheng, C., Li, M., Tang, R., Zhang, R., Lee, P. K. H., Lai, A. C. K., and  
410 Chan, C. K.: Sulfate Formation in Incense Burning Particles: A Single-Particle Mass Spectrometric Study, *Environmental*  
411 *Science & Technology Letters*, 9, 718-725, 10.1021/acs.estlett.2c00492, 2022a.
- 412 ^Liang, Z., Zhou, L., Infante Cuevas, R. A., Li, X., Cheng, C., Li, M., Tang, R., Zhang, R., Lee, P. K. H., Lai, A. C. K., and  
413 Chan, C. K.: Sulfate Formation in Incense Burning Particles: A Single-Particle Mass Spectrometric Study, *Environmental*  
414 *Science & Technology Letters*, 10.1021/acs.estlett.2c00492, 2022b.
- 415 ^Lin, T.-C., Yang, C.-R., and Chang, F.-H.: Burning characteristics and emission products related to metallic content in  
416 incense, *Journal of hazardous materials*, 140, 165-172, 2007.
- 417 ^Liu, T., Wang, Z., Huang, D. D., Wang, X., and Chan, C. K.: Significant Production of Secondary Organic Aerosol from  
418 Emissions of Heated Cooking Oils, *Environmental Science & Technology Letters*, 5, 32-37, 10.1021/acs.estlett.7b00530,  
419 2018.
- 420 ^Liu, T., Zhou, L., Liu, Q., Lee, B. P., Yao, D., Lu, H., Lyu, X., Guo, H., and Chan, C. K.: Secondary Organic Aerosol  
421 Formation from Urban Roadside Air in Hong Kong, *Environmental Science & Technology*, 53, 3001-3009,  
422 10.1021/acs.est.8b06587, 2019.
- 423 ^Lu, K., Fuchs, H., Hofzumahaus, A., Tan, Z., Wang, H., Zhang, L., Schmitt, S. H., Rohrer, F., Bohn, B., Broch, S., Dong, H.,  
424 Gkatzelis, G. I., Hohaus, T., Holland, F., Li, X., Liu, Y., Liu, Y., Ma, X., Novelli, A., Schlag, P., Shao, M., Wu, Y., Wu, Z.,  
425 Zeng, L., Hu, M., Kiendler-Scharr, A., Wahner, A., and Zhang, Y.: Fast Photochemistry in Wintertime Haze: Consequences  
426 for Pollution Mitigation Strategies, *Environ Sci Technol*, 53, 10676-10684, 10.1021/acs.est.9b02422, 2019.
- 427 ^Luo, J., Zhang, J., Huang, X., Liu, Q., Luo, B., Zhang, W., Rao, Z., and Yu, Y.: Characteristics, evolution, and regional  
428 differences of biomass burning particles in the Sichuan Basin, China, *Journal of Environmental Sciences*, 89, 35-46,  
429 <https://doi.org/10.1016/j.jes.2019.09.015>, 2020.
- 430 ^Lyu, X., Huo, Y., Yang, J., Yao, D., Li, K., Lu, H., Zeren, Y., and Guo, H.: Real-time molecular characterization of air  
431 pollutants in a Hong Kong residence: Implication of indoor source emissions and heterogeneous chemistry, *Indoor Air*, 31,  
432 1340-1352, <https://doi.org/10.1111/ina.12826>, 2021.



- 433 ^Mao, J., Ren, X., Brune, W., Olson, J., Crawford, J., Fried, A., Huey, L., Cohen, R., Heikes, B., and Singh, H.: Airborne  
434 measurement of OH reactivity during INTEX-B, *Atmospheric Chemistry and Physics*, 9, 163-173, 2009.
- 435 ^McFall, A. S., Johnson, A. W., and Anastasio, C.: Air–water partitioning of biomass-burning phenols and the effects of  
436 temperature and salinity, *Environmental Science & Technology*, 54, 3823-3830, 2020.
- 437 ^Neubauer, K. R., Johnston, M. V., and Wexler, A. S.: Humidity effects on the mass spectra of single aerosol particles,  
438 *Atmospheric Environment*, 32, 2521-2529, 1998.
- 439 ^Ng, N. L., Brown, S. S., Archibald, A. T., Atlas, E., Cohen, R. C., Crowley, J. N., Day, D. A., Donahue, N. M., Fry, J. L.,  
440 and Fuchs, H.: Nitrate radicals and biogenic volatile organic compounds: oxidation, mechanisms, and organic aerosol,  
441 *Atmospheric chemistry and physics*, 17, 2103-2162, 2017.
- 442 ^Peng, C. and Chan, C. K.: The water cycles of water-soluble organic salts of atmospheric importance, *Atmospheric*  
443 *Environment*, 35, 1183-1192, 2001.
- 444 ^Peng, X., Liu, X., Shi, X., Shi, G., Li, M., Liu, J., Huangfu, Y., Xu, H., Ma, R., Wang, W., and Feng, Y.: Source apportionment  
445 using receptor model based on aerosol mass spectra and 1 h resolution chemical dataset in Tianjin, China, *Atmospheric*  
446 *Environment*, 198, 387-397, <https://doi.org/10.1016/j.atmosenv.2018.11.018>, 2019.
- 447 ^Phares, D. J., Rhoads, K. P., Wexler, A. S., Kane, D. B., and Johnston, M. V.: Application of the ART-2a algorithm to laser  
448 ablation aerosol mass spectrometry of particle standards, *Analytical Chemistry*, 73, 2338-2344, 2001.
- 449 ^Qin, X. and Prather, K. A.: Impact of biomass emissions on particle chemistry during the California Regional Particulate Air  
450 Quality Study, *International Journal of Mass Spectrometry*, 258, 142-150, <https://doi.org/10.1016/j.ijms.2006.09.004>, 2006.
- 451 ^Ramazan, K., Wingen, L. M., Miller, Y., Chaban, G. M., Gerber, R. B., Xantheas, S. S., and Finlayson-Pitts, B. J.: New  
452 experimental and theoretical approach to the heterogeneous hydrolysis of NO<sub>2</sub>: Key role of molecular nitric acid and its  
453 complexes, *The Journal of Physical Chemistry A*, 110, 6886-6897, 2006.
- 454 ^Rissler, J., Vestin, A., Swietlicki, E., Fisch, G., Zhou, J., Artaxo, P., and Andreae, M. O.: Size distribution and hygroscopic  
455 properties of aerosol particles from dry-season biomass burning in Amazonia, *Atmos. Chem. Phys.*, 6, 471-491, 10.5194/acp-  
456 6-471-2006, 2006.
- 457 ^Rudich, Y., Donahue, N. M., and Mentel, T. F.: Aging of organic aerosol: Bridging the gap between laboratory and field  
458 studies, *Annu. Rev. Phys. Chem.*, 58, 321-352, 2007.
- 459 ^Schurman, M. I., Kim, J. Y., Cheung, H. H., and Chan, C. K.: Atmospheric particle composition-hygroscopic growth  
460 measurements using an in-series hybrid tandem differential mobility analyzer and aerosol mass spectrometer, *Aerosol Science*  
461 *and Technology*, 51, 694-703, 2017.
- 462 ^See, S. W. and Balasubramanian, R.: Characterization of fine particle emissions from incense burning, *Building and*  
463 *Environment*, 46, 1074-1080, <https://doi.org/10.1016/j.buildenv.2010.11.006>, 2011.
- 464 ^Seinfeld, J. and Pandis, S.: *Atmospheric chemistry and physics*. 1997, New York, 2008.
- 465 ^Sharma, V. K. and Graham, N. J. D.: Oxidation of Amino Acids, Peptides and Proteins by Ozone: A Review, *Ozone: Science*  
466 *& Engineering*, 32, 81-90, 10.1080/01919510903510507, 2010.



- 467 ^Sidibe, A., Sakamoto, Y., Murano, K., Sato, K., Yuba, A., Futami, M., Koita, O. A., Traore, I., and Kajii, Y.: Chemical  
468 Characterization and Health Risk Assessment of Particulate Matter from Household Activities in Bamako, Mali, Western Sub-  
469 Saharan Africa, *Atmosphere*, 13, 1290, 2022.
- 470 ^Silva, P. J. and Prather, K. A.: Interpretation of mass spectra from organic compounds in aerosol time-of-flight mass  
471 spectrometry, *Analytical Chemistry*, 72, 3553-3562, 2000.
- 472 ^Slade, J. H. and Knopf, D. A.: Multiphase OH oxidation kinetics of organic aerosol: The role of particle phase state and  
473 relative humidity, *Geophysical Research Letters*, 41, 5297-5306, 2014.
- 474 ^Spencer, M. T. and Prather, K. A.: Using ATOFMS to determine OC/EC mass fractions in particles, *Aerosol Science and*  
475 *Technology*, 40, 585-594, 2006.
- 476 ^Sullivan, R. C. and Prather, K. A.: Investigations of the diurnal cycle and mixing state of oxalic acid in individual particles  
477 in Asian aerosol outflow, *Environmental Science Technology*, 41, 8062-8069, 2007.
- 478 ^Taiwo, A. M., Harrison, R. M., Beddows, D. C., and Shi, Z.: Source apportionment of single particles sampled at the  
479 industrially polluted town of Port Talbot, United Kingdom by ATOFMS, *Atmospheric Environment*, 97, 155-165, 2014.
- 480 ^Volkamer, R., Jimenez, J. L., San Martini, F., Dzepina, K., Zhang, Q., Salcedo, D., Molina, L. T., Worsnop, D. R., and  
481 Molina, M. J.: Secondary organic aerosol formation from anthropogenic air pollution: Rapid and higher than expected,  
482 *Geophysical Research Letters*, 33, 2006.
- 483 ^Wang, B., Lee, S. C., and Ho, K. F.: Chemical composition of fine particles from incense burning in a large environmental  
484 chamber, *Atmospheric Environment*, 40, 7858-7868, <https://doi.org/10.1016/j.atmosenv.2006.07.041>, 2006.
- 485 ^Wang, X., Shen, Y., Lin, Y., Pan, J., Zhang, Y., Louie, P. K. K., Li, M., and Fu, Q.: Atmospheric pollution from ships and  
486 its impact on local air quality at a port site in Shanghai, *Atmos. Chem. Phys.*, 19, 6315-6330, 10.5194/acp-19-6315-2019,  
487 2019.
- 488 ^Xia, N., Du, E., Guo, Z., and de Vries, W.: The diurnal cycle of summer tropospheric ozone concentrations across Chinese  
489 cities: Spatial patterns and main drivers, *Environmental Pollution*, 286, 117547, <https://doi.org/10.1016/j.envpol.2021.117547>,  
490 2021.
- 491 ^Xiao, H. W., Zhu, R. G., Pan, Y. Y., Guo, W., Zheng, N. J., Liu, Y. H., Liu, C., Zhang, Z. Y., Wu, J. F., and Kang, C. A.:  
492 Differentiation between nitrate aerosol formation pathways in a southeast Chinese city by dual isotope and modeling studies,  
493 *Journal of Geophysical Research: Atmospheres*, 125, e2020JD032604, 2020.
- 494 ^Xu, J., Wang, H., Li, X., Li, Y., Wen, J., Zhang, J., Shi, X., Li, M., Wang, W., Shi, G., and Feng, Y.: Refined source  
495 apportionment of coal combustion sources by using single particle mass spectrometry, *Science of The Total Environment*, 627,  
496 633-646, <https://doi.org/10.1016/j.scitotenv.2018.01.269>, 2018.
- 497 ^Yabushita, A., Enami, S., Sakamoto, Y., Kawasaki, M., Hoffmann, M., and Colussi, A.: Anion-catalyzed dissolution of NO<sub>2</sub>  
498 on aqueous microdroplets, *The Journal of Physical Chemistry A*, 113, 4844-4848, 2009.
- 499 ^Yao, X., Fang, M., and Chan, C. K.: Size distributions and formation of dicarboxylic acids in atmospheric particles,  
500 *Atmospheric Environment*, 36, 2099-2107, 2002.



- 501 ^Yao, Y., Xie, Y., Zhao, B., Zhou, L., Shi, Y., Wang, Y., Sheng, Y., Zhao, H., Sun, J., and Cao, H.: N-dependent ozonation  
502 efficiency over nitrogen-containing heterocyclic contaminants: A combined density functional theory study on reaction  
503 kinetics and degradation pathways, *Chemical Engineering Journal*, 382, 122708, <https://doi.org/10.1016/j.cej.2019.122708>,  
504 2020.
- 505 ^Ye, C., Chen, R., and Chen, M.: The impacts of Chinese Nian culture on air pollution, *Journal of Cleaner Production*, 112,  
506 1740-1745, 2016.
- 507 ^Zaveri, R. A., Shilling, J. E., Zelenyuk, A., Liu, J., Bell, D. M., D'Ambro, E. L., Gaston, C. J., Thornton, J. A., Laskin, A.,  
508 and Lin, P.: Growth kinetics and size distribution dynamics of viscous secondary organic aerosol, *Environmental science &*  
509 *technology*, 52, 1191-1199, 2018.
- 510 ^Zhai, J., Wang, X., Li, J., Xu, T., Chen, H., Yang, X., and Chen, J.: Thermal desorption single particle mass spectrometry of  
511 ambient aerosol in Shanghai, *Atmospheric Environment*, 123, 407-414, 2015.
- 512 ^Zhang, G., Lian, X., Fu, Y., Lin, Q., Li, L., Song, W., Wang, Z., Tang, M., Chen, D., Bi, X., Wang, X., and Sheng, G.: High  
513 secondary formation of nitrogen-containing organics (NOCs) and its possible link to oxidized organics and ammonium, *Atmos.*  
514 *Chem. Phys.*, 20, 1469-1481, 10.5194/acp-20-1469-2020, 2020.
- 515 ^Zhang, S., Wang, Z., Zhang, J., Guo, D., and Chen, Y.: Inhalable cigarette-burning particles: Size-resolved chemical  
516 composition and mixing state, *Environmental Research*, 202, 111790, 2021.
- 517 ^Zhang, X., Xu, J., Zhai, L., and Zhao, W.: Characterization of Aerosol Properties from the Burning Emissions of Typical  
518 Residential Fuels on the Tibetan Plateau, *Environmental Science & Technology*, 10.1021/acs.est.2c04211, 2022a.
- 519 ^Zhang, X., Xu, J., Zhai, L., and Zhao, W.: Characterization of Aerosol Properties from the Burning Emissions of Typical  
520 Residential Fuels on the Tibetan Plateau, *Environmental Science & Technology*, 56, 14296-14305, 10.1021/acs.est.2c04211,  
521 2022b.
- 522 ^Zhang, Y., Zhang, X., Sun, J., Hu, G., Shen, X., Wang, Y., Wang, T., Wang, D., and Zhao, Y.: Chemical composition and  
523 mass size distribution of PM<sub>1</sub> at an elevated site in central east China, *Atmospheric Chemistry and Physics*, 14, 12237-12249,  
524 2014.
- 525 ^Zhao, Z.-Y., Cao, F., Fan, M.-Y., Zhai, X.-Y., Yu, H.-R., Hong, Y., Ma, Y.-J., and Zhang, Y.-L.: Nitrate aerosol formation  
526 and source assessment in winter at different regions in Northeast China, *Atmospheric Environment*, 267, 118767, 2021.
- 527 ^Zhou, Y., Wang, Z., Pei, C., Li, L., Wu, M., Wu, M., Huang, B., Cheng, C., Li, M., Wang, X., and Zhou, Z.: Source-oriented  
528 characterization of single particles from in-port ship emissions in Guangzhou, China, *Science of The Total Environment*, 724,  
529 138179, <https://doi.org/10.1016/j.scitotenv.2020.138179>, 2020.
- 530 ^Zuend, A., Marcolli, C., Luo, B. P., and Peter, T.: A thermodynamic model of mixed organic-inorganic aerosols to predict  
531 activity coefficients, *Atmos. Chem. Phys.*, 8, 4559-4593, 10.5194/acp-8-4559-2008, 2008.
- 532